Journal of Geophysical Research Atmospheres

Supporting Information for

Sources, Occurrence and Characteristics of Fluorescent Biological Aerosol Particles Measured over the Pristine Southern Ocean

Alireza Moallemi[1], Sebastian Landwehr[1,2], Charlotte Robinson[3], Rafel Simó[4], Marina Zamanillo[4], Gang Chen[1], Andrea Baccarini[1,2], Martin Schnaiter[5,6], Silvia Henning[7], Robin L. Modini[1,*], Martin Gysel-Beer[1], and Julia Schmale[1,2,*]

1. Laboratory of Atmospheric Chemistry, Paul Scherrer Institute, Villigen PSI, 5232, Switzerland

2. Extreme Environments Research Laboratory, École Polytechnique Fédérale de Lausanne, School of Architecture, Civil and Environmental Engineering, Lausanne, Switzerland

3. Remote Sensing and Satellite Research Group, Curtin University, Kent Street, Bentley 6102 WA, Australia

4. Institut de Ciències del Mar, ICM-CSIC, Pg Marítim de la Barceloneta 37-49, 08003 Barcelona, Catalonia, Spain

5. Institut für Meteorologie und Klimaforschung, Karlsruher Institut für Technologie, Karlsruhe, Germany

6. schnaiTEC GmbH, Karlsruhe, Germany

7. Institute for Tropospheric Research, Department of Physics, Leipzig, Germany

Corresponding authors: Robin L. Modini (robin.modini@psi.ch) and Julia Schmale (julia.schmale@epfl.ch)

Contents of this file

Introduction

This supporting document contains information on the analysis of wide band integrated bioaerosol senor data, complementary results related to fluorescent and hyper-fluorescent aerosol number concentration, description of marine biological and chemical measurements, and further details regarding ABC fluorescent classification of aerosol particles. Moreover, the document contains scatter plots of (hyper-)fluorescent particle fractions against marine biological and chemical variables. The results demonstrated here were acquired during the Antarctic Circumnavigation Expedition (ACE) in austral summer 2016-2017.

Text S1: Missing Particle Count Fraction

To show the contribution of the missing particle counts by the WIBS, the fraction of missed particle counts (MPC) to the total detected particles particle number (Ntot) are is presented in Figure S1. These results indicate that the median of the fraction of missing particle counts ranges from ~ 5 to 8 %.

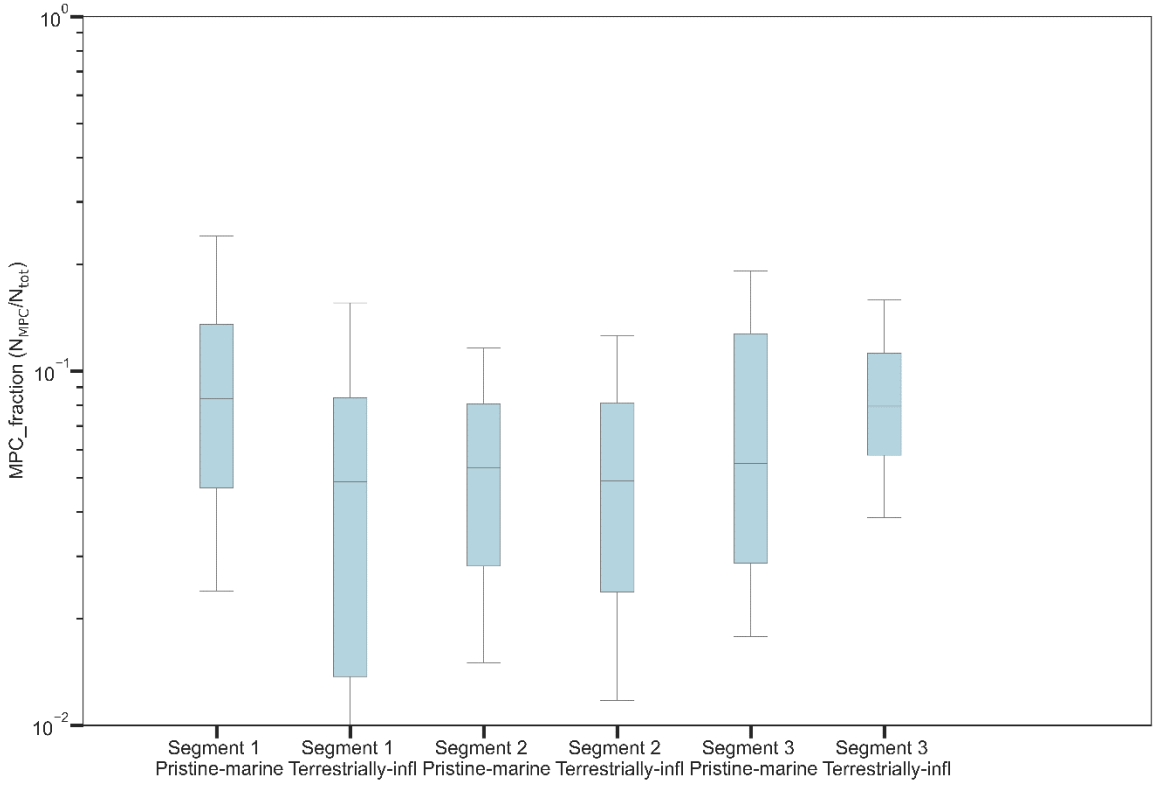

Figure S1. Variation of the fraction of missing particle count to total particle number concentration measured by the WIBS.

Text S2: APS vs WIBS coarse mode aerosol measurements

Figure S2 shows the scatter plot of hourly averaged integrated number concentrations of total aerosol particles measured by APS and WIBS for particles within the size range of 1 µm to 20 µm, for samples collected in segments 1-3 of ACE and samples collected after segment 3 during the return route from Cape Town to Europe.

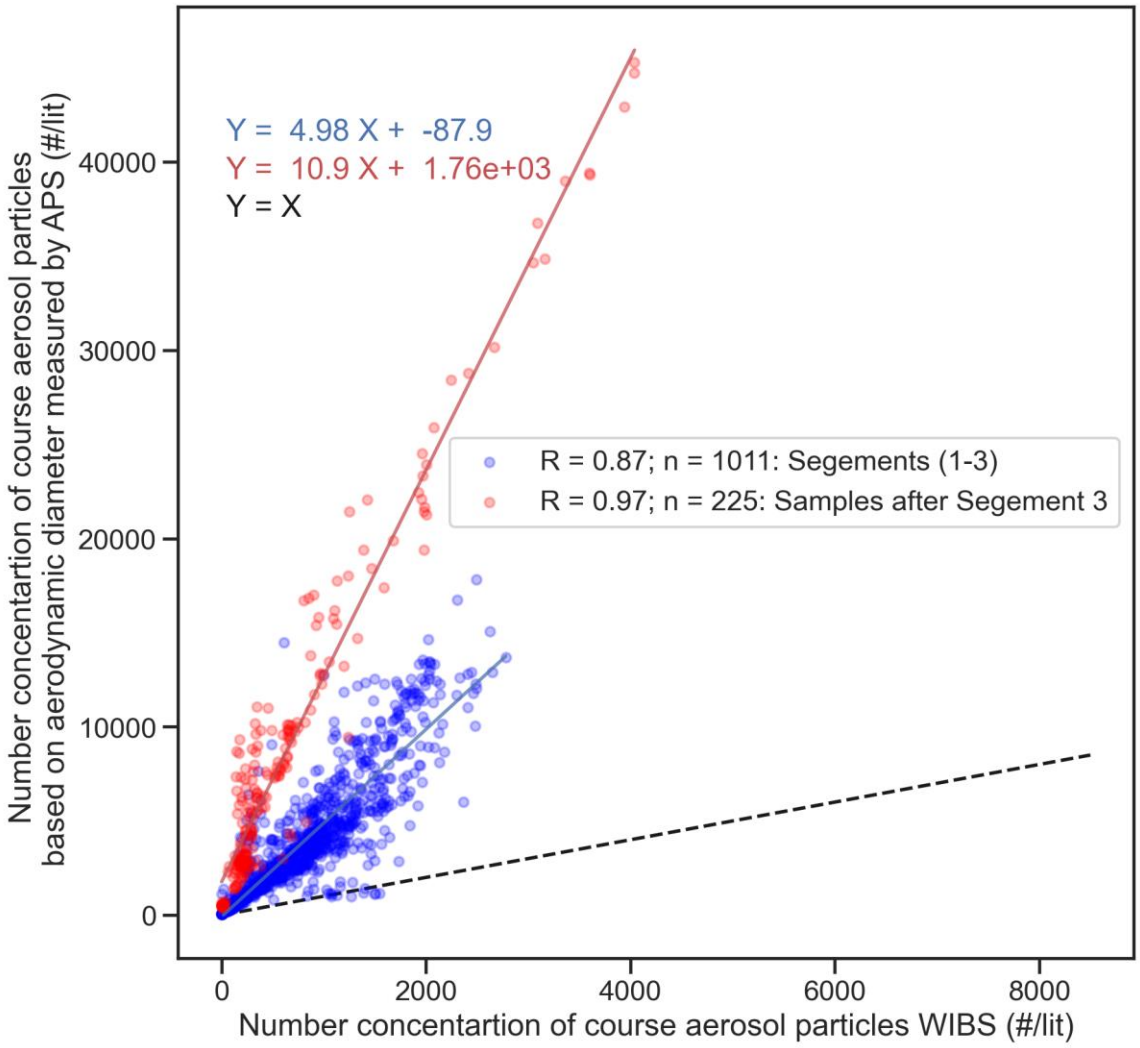

Figure S2. Comparison of particle number concentrations for the diameter range 1 – 20 µm obtained with the WIBS and APS, for samples collected during segments 1-3 and samples collected after segment 3. The correlation coefficient (R) included in the plot corresponds to Pearson's correlation coefficient.

Text S3: Marine Measurement Description

In this section, marine variables and their analysis methods are presented.

Table S1. Description of marine microbe measurement used in the correlation study against fluorescent aerosol particles.

Variable	Units	Description	Methods
HDNA_bacteria-sea-p8	Cells mL^{-1}	Concentration of high DNA containing bacteria	See section S 4.1
LDNA_bacteria-sea-p8	Cells mL^{-1}	Concentration of low DNA containing bacteria	See section S 4.1
Total-bacteria-sea	Cells mL^{-1}	Concentration of total bacteria (high & low DNA containing) bacteria	See section S 4.1
Synechococcus-sea-p8	Cells mL^{-1}	Concentration of *Synechoccocus* sp. Cells	See section S 4.1
Picoeukaryotes-type1-sea-p8	Cells mL^{-1}	Concentration of picoeukaryote type 1 cells	See section S 4.1
Picoeukaryotes-type2-sea-p8	Cells mL^{-1}	Concentration of picoeukaryote type 2 cells	See section S 4.1
Nanoeukaryotes-sea-p8	Cells mL^{-1}	Concentration of nanoeukaryote cells	See section S 4.1
Cryptomonas-sea-p8	Cells mL^{-1}	Concentration of cryptomonas cells	See section S 4.1
Picoeukaryotes-sea-p8	Cells mL^{-1}	Concentration of picoeukaryote (type 1 & type 2) cells	See section S 4.1

Table S2. Description of marine phytoplankton taxa measurements used in the correlation study against fluorescent aerosol particles

Variable	Units	Description	Methods
Particulate.Org.Carbon-p1	μM	Particulate organic carbon concentration	See section S 4.2
Total_Chlorophyll_a_merged-p1	$\mu g\ L^{-1}$	Total chlorophyll-a concentration	See section S 4.3
Chloro	$\mu g\ L^{-1}$	chlorophyte contribution to chlorophyll biomass	See section S 4.4
Crypto1	$\mu g\ L^{-1}$	Cryptophyte contribution to chlorophyll biomass	See section S 4.4
Cyano2	$\mu g\ L^{-1}$	Cyanobacteria type 2 contribution to chlorophyll biomas	See section S 4.4
DiatA	$\mu g\ L^{-1}$	Diatom type contribution to chlorophyll biomas	See section S 4.4
DiatB	$\mu g\ L^{-1}$	Diatom type 2 contribution to chlorophyll biomas	See section S 4.4
DinoA	$\mu g\ L^{-1}$	Dinoflagellate type 1 contribution to chlorophyll biomas	See section S 4.4
Hapto8	$\mu g\ L^{-1}$	Haptophyte type 8 contribution to chlorophyll biomas	See section S 4.4
Haptophyte67	$\mu g\ L^{-1}$	Haptophyte type 6&7 contribution to chlorophyll biomas	See section S 4.4
Pras3	$\mu g\ L^{-1}$	Prasinophyte type 3 contribution to chlorophyll biomas	See section S 4.4
Pelago	$\mu g\ L^{-1}$	Pelagophyte contribution to chlorophyll biomas	See section S 4.4

Table S3. Description of other marine organic measurements.

Dissolved Compounds			
Variable	Units	Description	Methods
CDOM_abs_350nm	m^{-1}	Colored dissolved organic material (CDOM) absorption at 350 nm	See section S 4.5
TEP	µg XG eq L^{-1}	Transparent Exopolymeric Particles	See section S 4.6
CSP	µg BSA eq L^{-1}	Coomasie Stainable Particles	See section S 4.6

Text S4: Description of methods used for marine measurement

S4.1 Marine microbe number concentration measurements

Number concentration of bacteria and pico-, nano- and microalgae in sea water were measured through cytometry. After extraction, sea water samples were aliquoted in cryovials. For each samples 4.5 ml duplicates and 1.8 ml replicate were collected. The samples were treated by 1% paraformaldehyde plus 0.05% glutaraldehyde and kept at – 80 ˚C until analysis on land. After thawing, samples were analysed with a PARTEC Cube 8 flow cytometer equipped with a laser emitting at 488 nm. Heterotrophic bacteria were counted by their signature in a plot of side scatter versus green fluorescence after being stained with 10 µM of SYBRGreen I. In separate runs of unstained samples, pico- and nano-phytoplankton and cryptomonas cells were identified and enumerated on the basis of the differences in autofluorescence and light scattering characteristics.

S4.2 Particulate organic carbon concentration measurements

Particulate organic carbon was measured by extracting 2000 ml of sea water samples and filtering them using 25 mm combusted 0.3 µm Glass Fibre filters (GF-75; Sterlitech). After sample extraction, the filter papers were kept in combusted tinfoil and cooled down to -80 °C. The filters were analyzed in University of Cape Town using an elemental analyser-isotope ratio mass spectrometer (Walton and Thomas, 2018). The particulate organic carbon data could be found in (Thomalla et al., 2020).

S4.3 Merged total chlorophyll-a

Absolute concentrations of total chlorophyll-a pigment concentration were derived via high performance liquid chromatography (HPLC, Antoine et al., 2019) at locations roughly every 6-12 hours. Measurements of particulate absorption were collected at a higher resolution, roughly every 3-6 hours. Using matched samples of HPLC derived total chlorophyll-a and particulate absorption, the absorption line height method of Roesler & Barnard (2013) for determining total chlorophyll-a concentration was calibrated and applied to the whole particulate absorption dataset in order to increase the resolution of the total chlorophyll-a concentration estimations

S4.4 Phytoplankton CHEMTAX

The data on phytoplankton taxonomy groups and their contributions were obtained from the pigment concentration measurements (Antoine et al., 2019) and by using

CHEMTAX v1.95 chemical taxonomy software (Mackey et al., 1996). The quantified taxonomy groups in this studies are: Chlorophytes type 1, cryptophytes type 2, diatoms type 1, diatoms type 2, dinoflagellates type 1, haptophytes type 8, haptophytes types 6 + 7, prasinophytes, and pelagophytes (Higgins at al., 2011). Before conducting CHEMTAX analysis, the data was pre-processed and clustered. The data was standardized was based on mean subtracted and divided by standard deviation. Prior to clustering the data, a dissimilarity matrix was computed based Manhattan's distances. Hierarchical clustering (Ward's method) was used for clustering analysis and the Elbow, silouette and gap tests indicated the existence of 5 clusters. The CHEMTAX analysis was conducted on the clustered data. Initially, to obtain the matrices of optimized pigment rations, 60 analysis runs were performed on each individual clustered. This was followed by a final 20 analysis runs on the data to calculate the taxonomic abundance. In this study the initial pigment ratios were gathered from Rodriguez et al. (2002) (2002), Zapata et al. (2004), Cook et al. (2011) and Higgins at al. (2011), Cassar et al. (2015), Nunes et al. (2019).

S4.5 Coloured dissolved organic matter (CDOM) concentration measurements

Coloured dissolved organic matter is a component dissolved organic matter (DOM) in seaweter which strongly absorbs light in the ultraviolet wavelengths. CDOM is typically strongly correlated with DOM and could be used as a proxy for DOM. The absorption spectra of the CDOM from the collected sample were measured onboard with a UV-spectrometer, and the data included in this analysis corresponds to the absorption of CDOM at wavelength of 350 nm. Further information can be found in the cruise report (Walton and Thomas, 2018).

S4.6 Transparent Exopolymeric Particles (TEPs) and Coomasie Stainable Particles (CSPs) measurements

Transparent exopolymeric particles (TEP) and coomassie-blue stainable particles (CSP) are gel-like compounds that are rich in polysaccharide and protein, respectively. Seawater samples (150-300 ml) were filtered through 25 mm diameter 0.4 µm pore size polycarbonate filters. For TEP analysis the filters were stained with 500 µL of Alcian blue solution (0.02 %, pH 2.5) for 5 s, rinsed with Milli-Q water and stored frozen. For CSP analysis, the filters were stained with 700 µL of a working Coomassie Brilliant Blue (CBB-G 250) solution (0.04 %, pH 7.4) for 30 s, rinsed with Milli-Q water and stored frozen. For each batch of TEP and CSP samples duplicate blank filters which were not stained were collected. Measurements of TEP and CSP were conducted in land laboratories. For TEP all the samples and blank filters were treated in 5 ml of 80% sulfuric acid and shaken intermittently for 3 h. The measurement was conducted by a spectrophotometre at 787 nm (Varian Cary spectrophotometer). For CSP all the samples and blank filters were treated in 4 mL of extraction solution (3 % SDS in 50 % isopropyl alcohol) and sonicated in a water bath at 37^{o} C for 2 hours. The CSP measurement was conducted y a spectrophotometre at 615 nm (Shimadzu UV–Vis UV120). The Alcian blue dye solution calibration was performed using a standard

solution of Xanthan Gum (XG). The CBB dye solution calibration was performed using bovine serum albumin standard (BSA).

Text S5: Correlation analysis of SSA proxies vs fluorescent aerosols at different land proximity values

To find a reasonable proximity to land distance, the Pearson's R values of the different proxy variables against fluorescent and hyper-fluorescent coarse particles were obtained as a function of the distance to land. Figures S3 and S4 show the results for fluorescent and hyper-fluorescent particles, respectively.

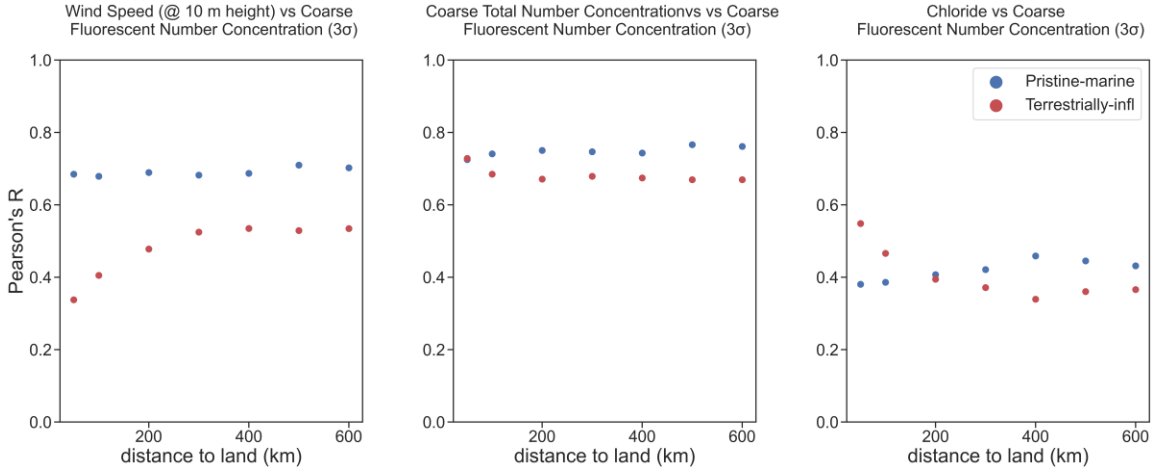

Figure S3. Pearson's R values for pristine-marine and terrestrially-influenced air masses of fluorescent particles for different land proximity values.

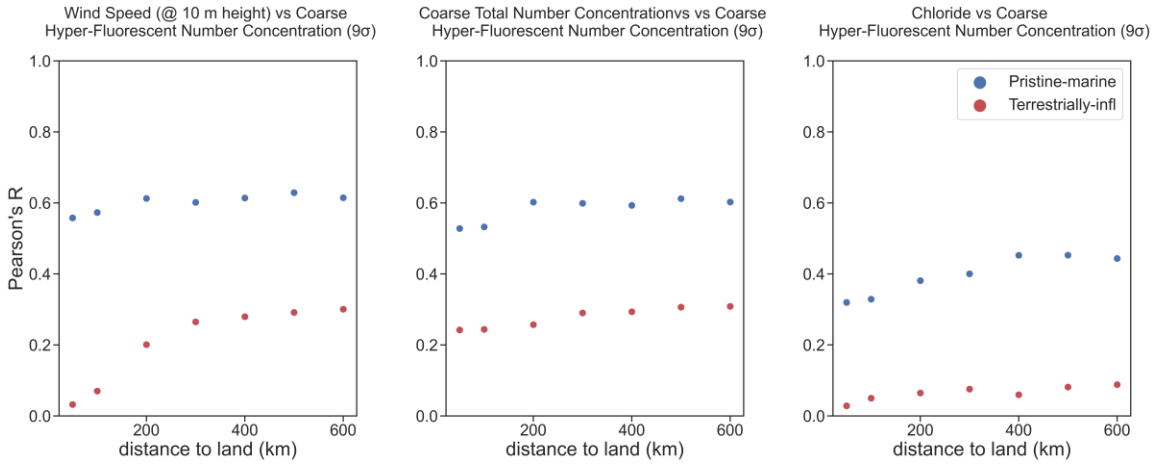

163

164 **Figure S4.** Pearson's R values for pristine-marine and terrestrially-influenced air masses of
165 hyper-fluorescent particles for different land proximity values.

166 **Text S5: Scatterplots of fluorescent particle (3σ) concentrations against the four**
167 **proxy variables for SSA concentrations**

168 The scatter plots for fluorescent coarse particles vs SSA proxies are presented in Figure

169 S5.

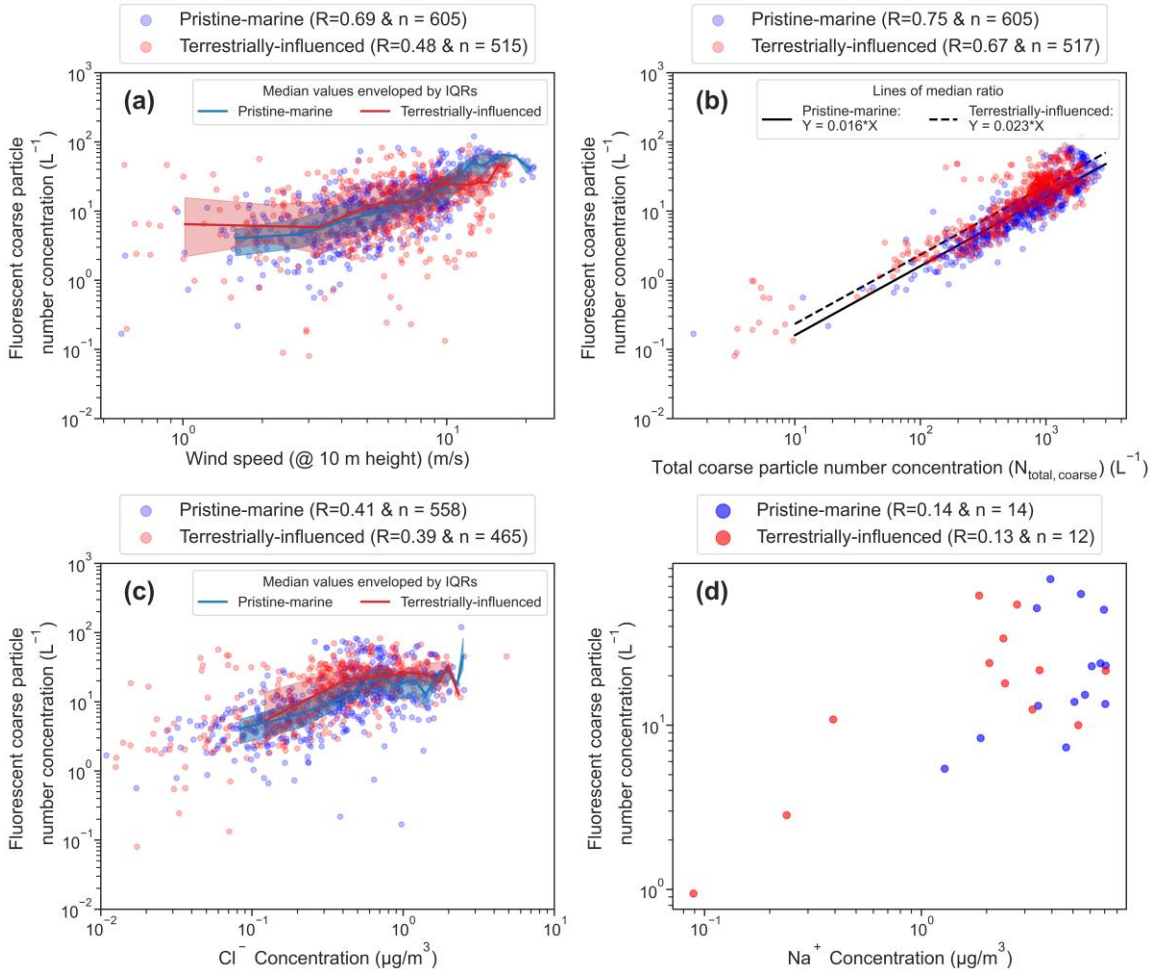

Figure S5. Scatter plots of pristine-marine and terrestrially-influenced air masses of fluorescent particles vs SSA proxies for the combined segment 1 to segment 3 results. The red and blue shades correspond to the interquartile ranges (IQR) of the measurements that were calculated by binning the dataset into ten equidistant logarithmic bins.

Text S6: Distribution of the number concentration fraction of fluorescent PBAPs to coarse SSA number concentrations

The histograms of the fraction of (hyper-)fluorescent number concentrations to total coarse aerosol particle number concentrations based on hourly averaged data are shown in Figures S6 and S7.

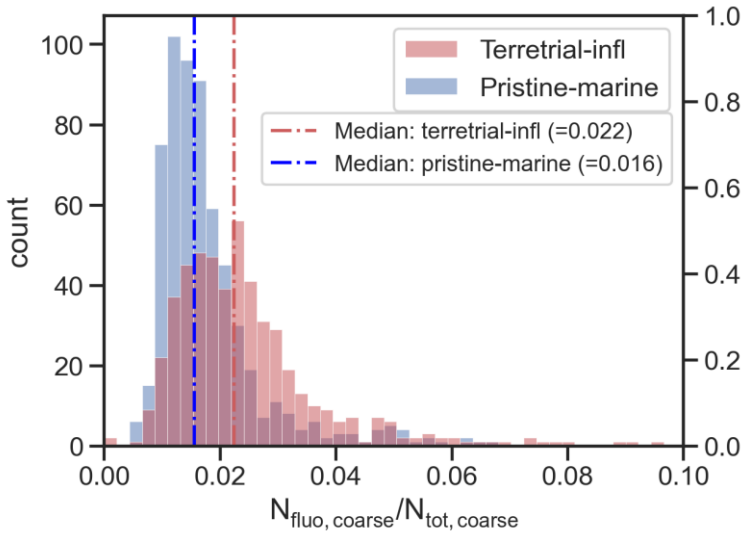

182

183 **Figure S6.** Distribution of number fraction of fluorescent PBAP to total coarse particle number
184 concentration.

185

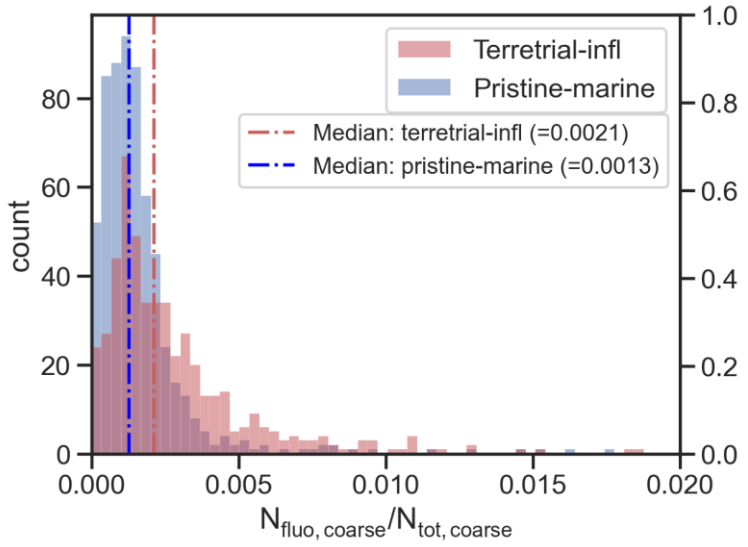

186

187 **Figure S7.** Distribution of number fraction of hyper-fluorescent PBAP to total coarse particle
188 number concentration.

189

Text S7: Scatter plots of different marine variables against normalized fluorescent number concentration

S7.1 Fluorescent particle number concentration fraction vs phytoplankton taxa

Figures S8 and S9 show the results of the fraction of coarse fluorescent particle number concentrations to total coarse particles against marine measurements associated with phytoplankton taxa. All the fit lines in the plots demonstrated in section S7 correspond to linear regressions that were applied on the datasets. The Pearson's R values are also included.

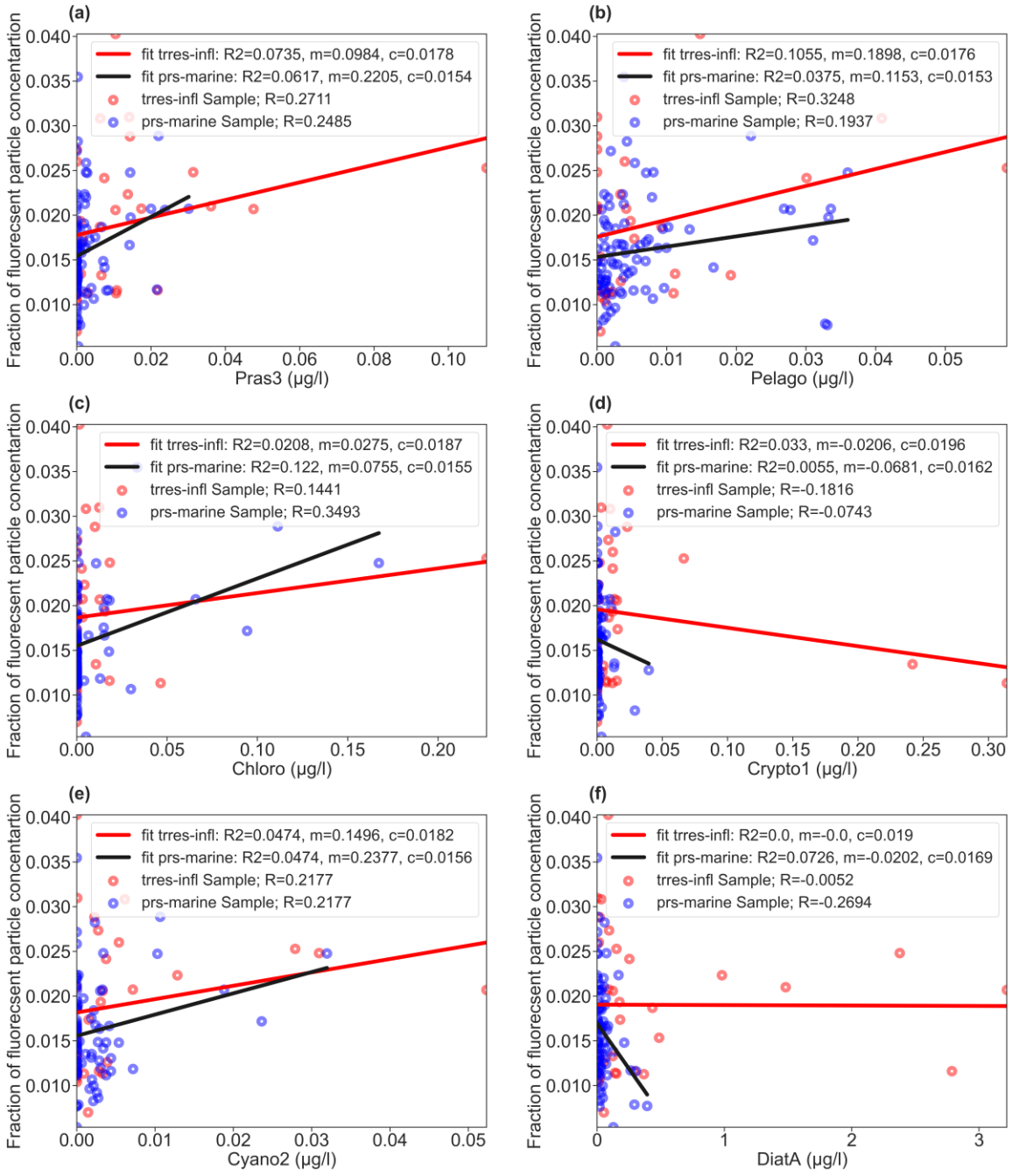

198

199 **Figure S8.** Scatter plot of fraction of coarse fluorescent particle number concentrations to
200 total coarse particles vs. different phytoplankton taxa measurements.

201

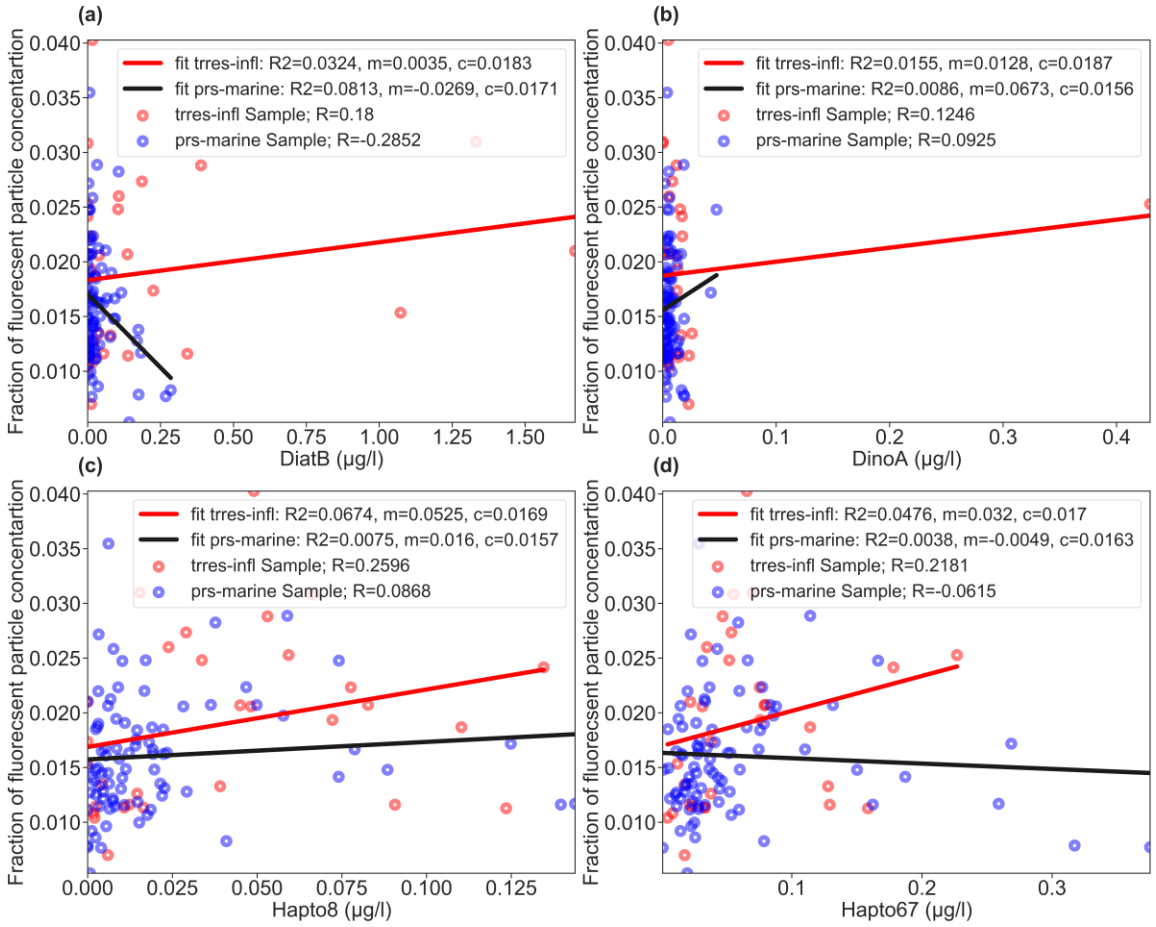

Figure S9. Scatter plot of fraction of coarse fluorescent particle number concentrations to total coarse particles vs. different phytoplankton taxa measurements

S7.2 Fluorescent particle number concentration fraction vs marine microbe measurements

Figures S10 and S11 show the results of the fraction of coarse fluorescent particle number concentrations to total coarse particles against marine measurements associated with marine microbe measurements. Fits are analogue to S 9.1.

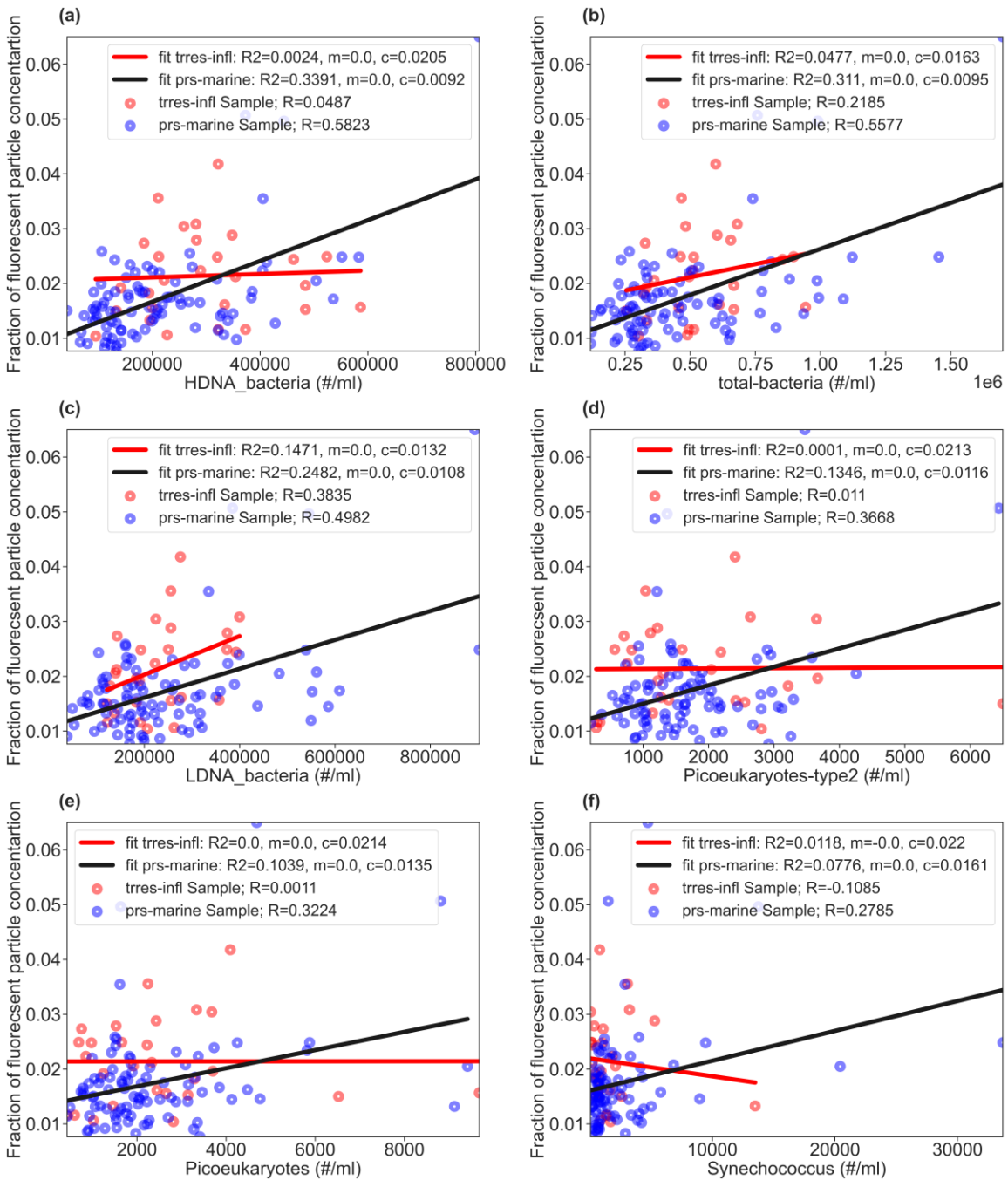

213

214 **Figure S10.** Scatter plot of fraction of coarse fluorescent particle number concentrations to
215 total coarse particles vs. different marine microbe measurements

216

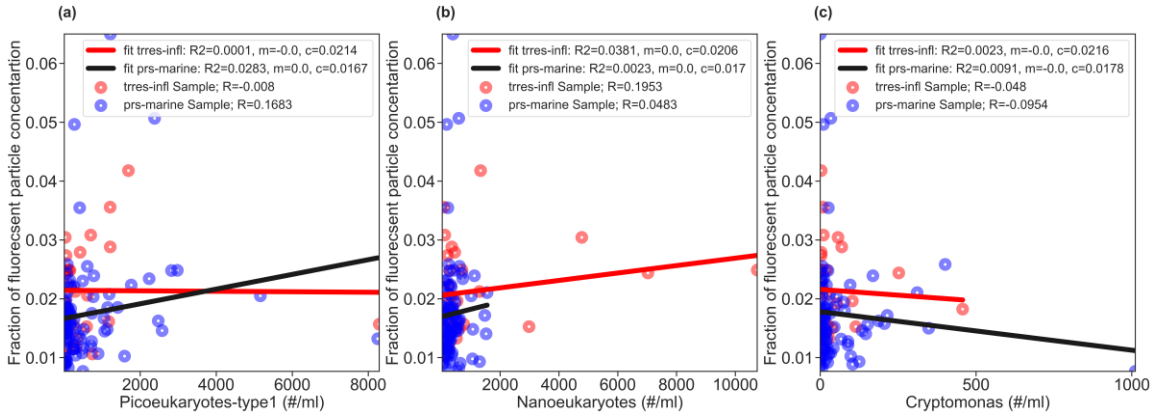

Figure S11. Scatter plot of fraction of coarse fluorescent particle number concentrations to total coarse particles vs. different marine microbe measurements

S7.3 Fluorescent particle number concentration fraction vs organic matter (OM) measurements

Figure S12 shows the results of fraction of coarse fluorescent particle number concentrations to total coarse particles against OM measurements. Fits are analogue to S 9.1.

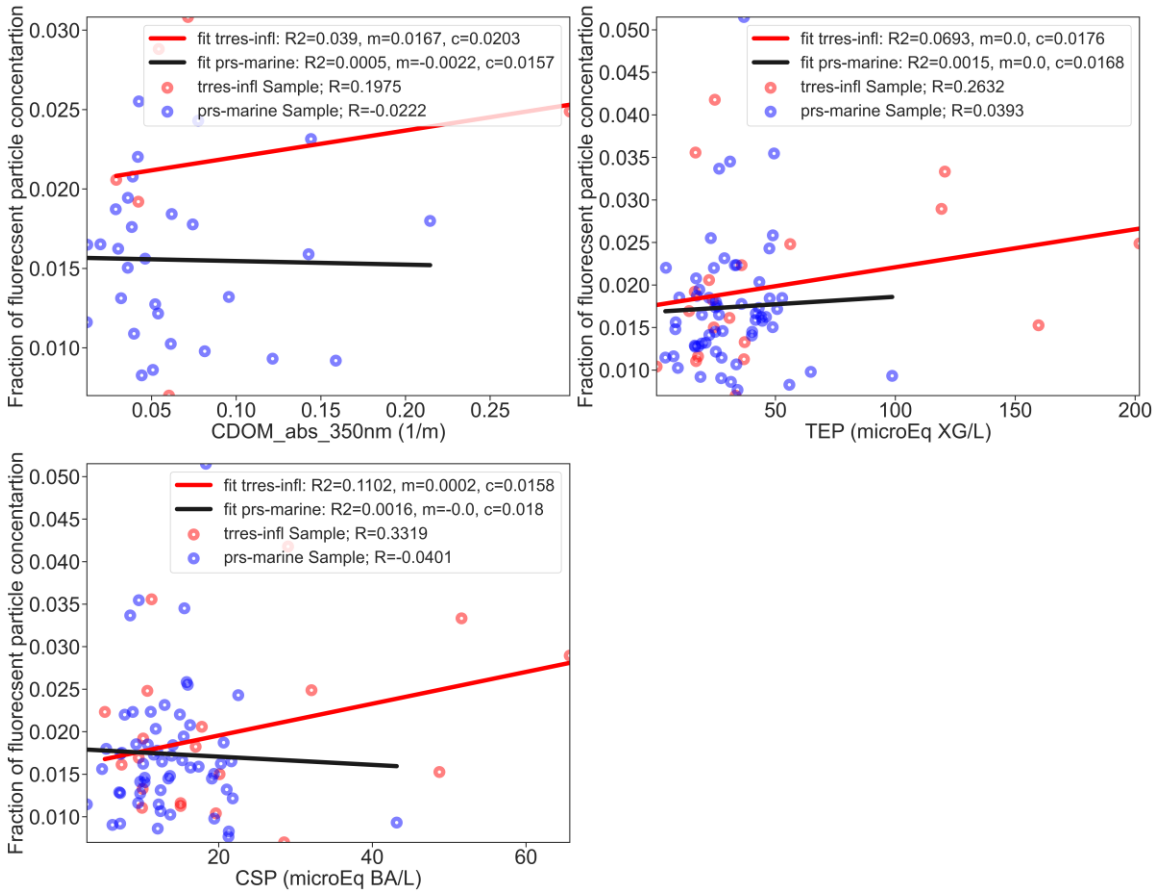

227

228 **Figure S12.** Scatter plot of fraction of coarse fluorescent particle number concentrations to
229 total coarse particles vs. OM measurements.

230

231

232 ***S7.4 Hyper-fluorescent particle number concentration fraction vs phytoplankton taxa***

233 Figures S13 and S14 show the scatter results of fraction of coarse hyper-fluorescent

234 particle number concentrations to total coarse particles against marine measurements

235 associated with phytoplankton taxa.

236

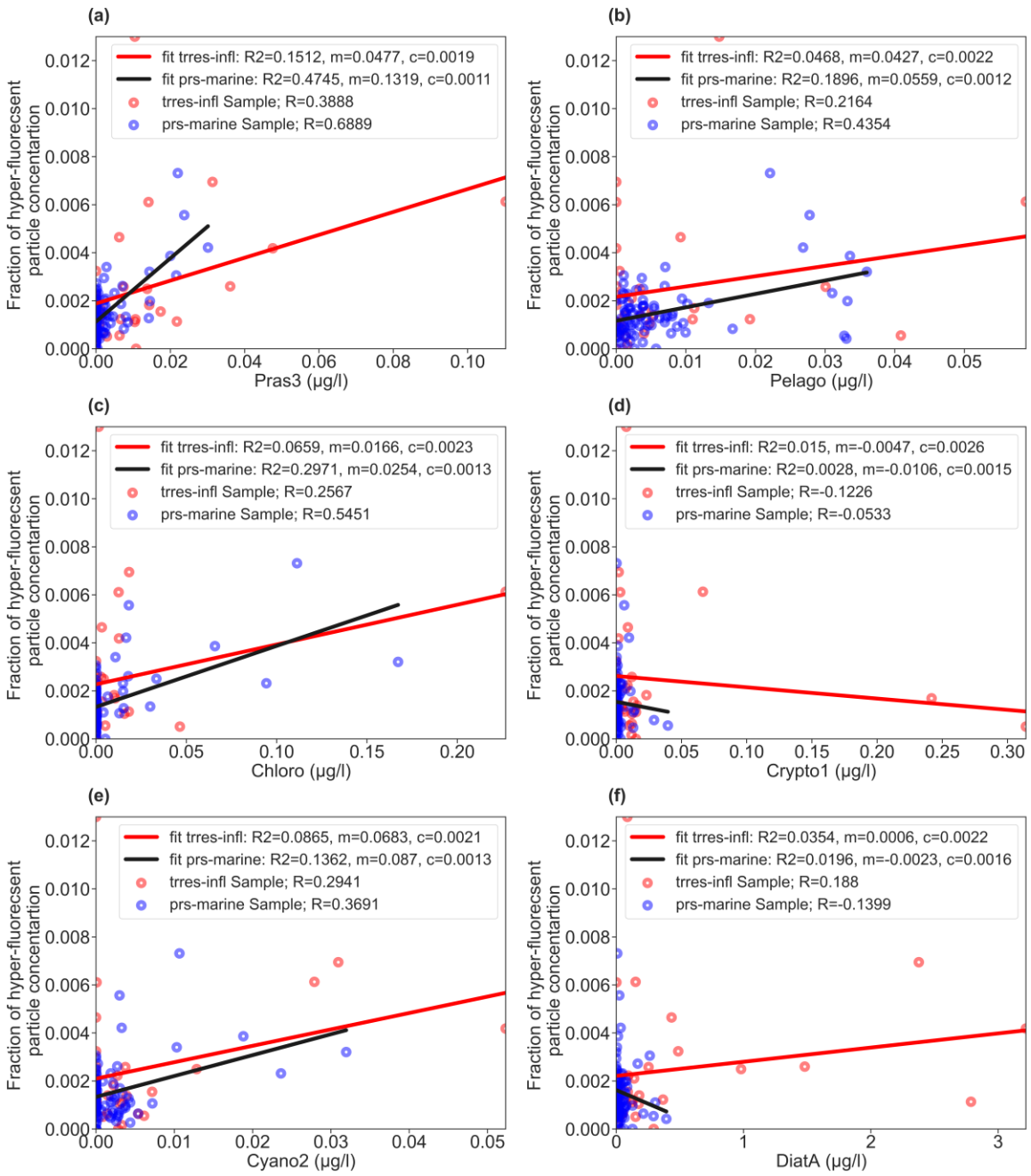

Figure S13. Scatter plot of fraction of coarse hyper-fluorescent particle number concentrations to total coarse particles vs. different phytoplankton taxa measurements

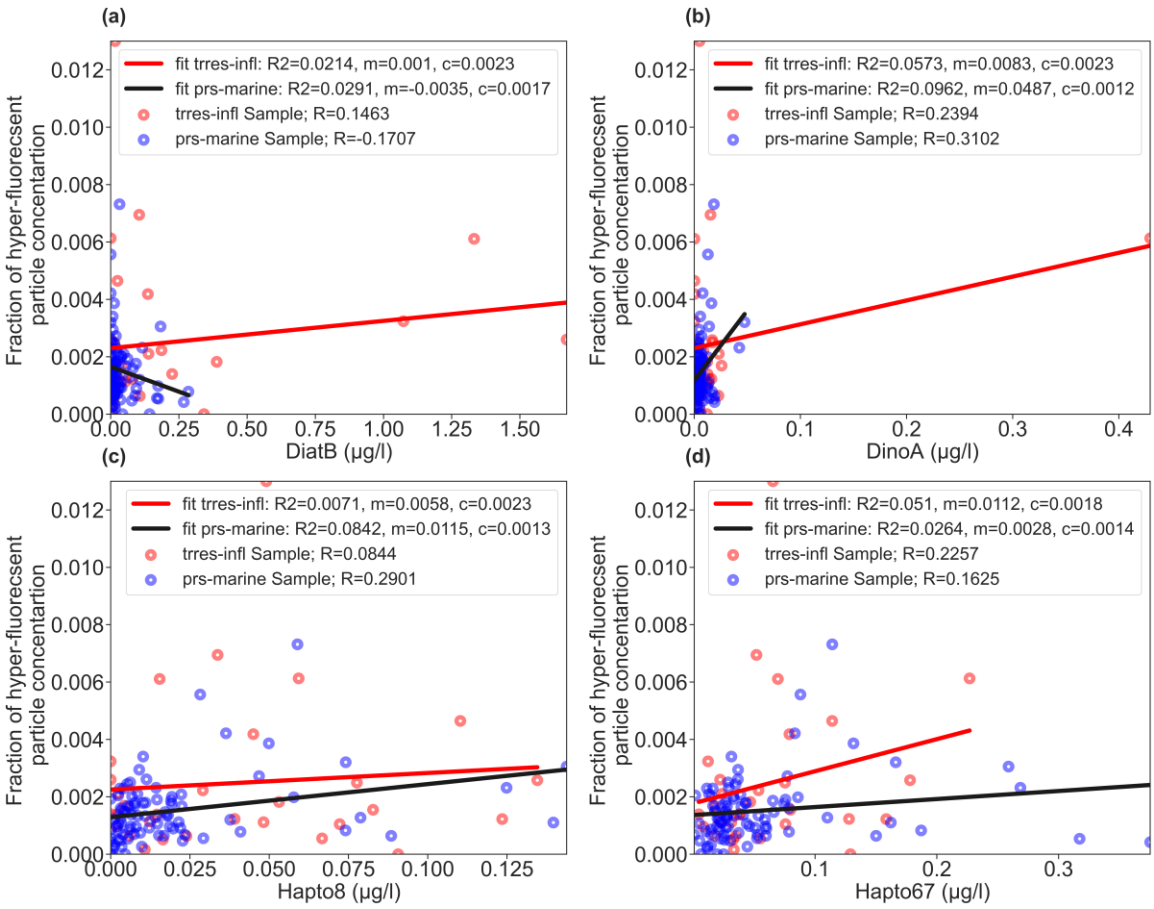

Figure S14. Scatter plot of fraction of coarse hyper-fluorescent particle number concentrations to total coarse particles vs. different phytoplankton taxa measurements

S7.5 Hyper-fluorescent particle number concentration fraction vs marine microbe measurements

Figures S15 and S16 show the scatter results of fraction of coarse hyper-fluorescent particle number concentrations to total coarse particles against marine measurements associated with marine microbe measurements.

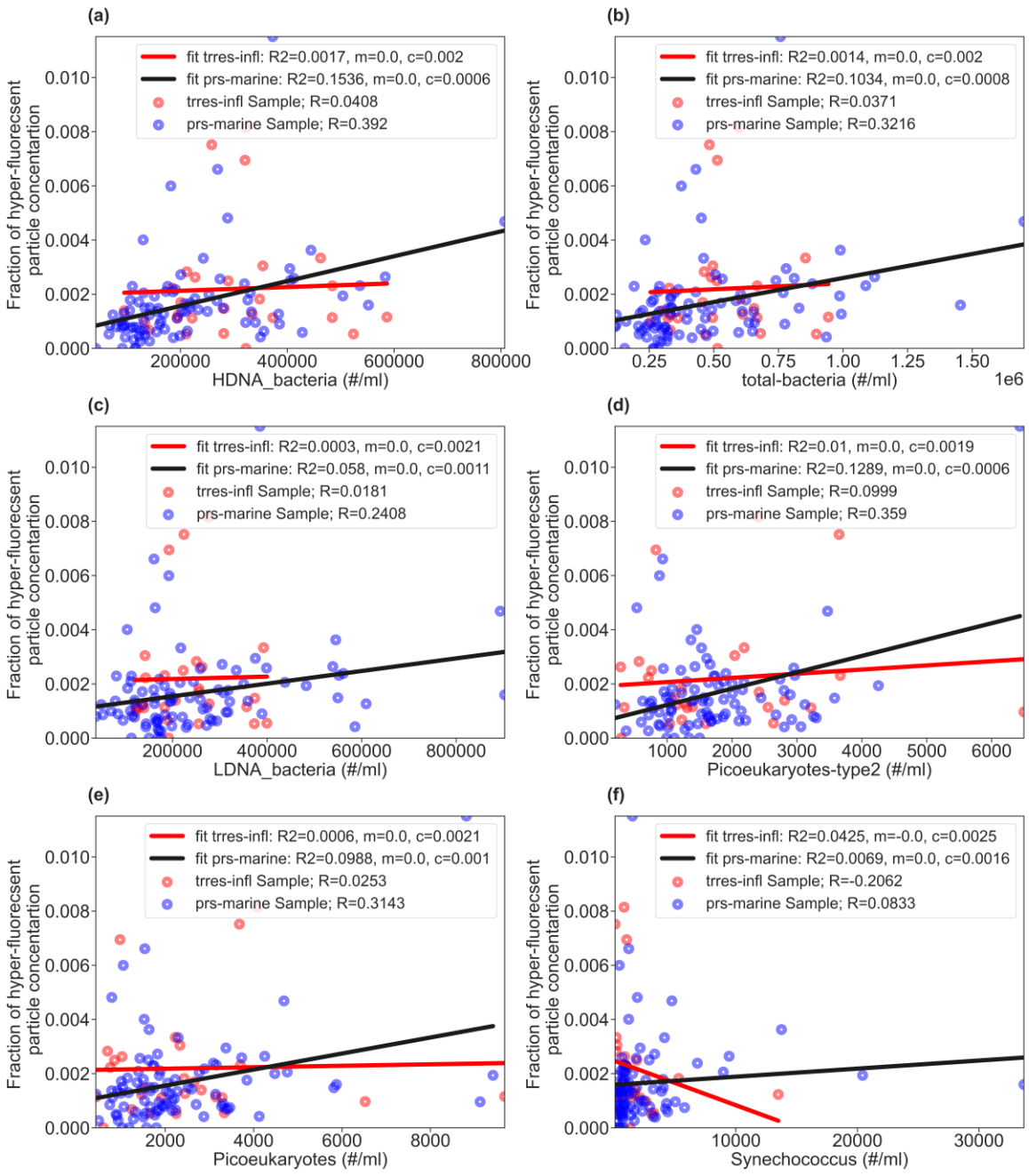

253

254 **Figure S15.** Scatter plot of fraction of coarse hyper-fluorescent particle number
255 concentrations to total coarse particles vs. different marine microbe measurements

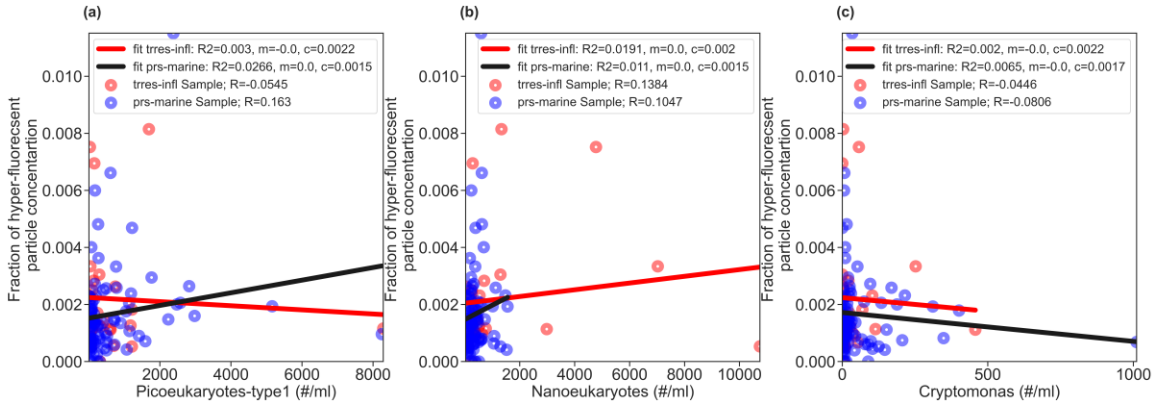

Figure S16. Scatter plot of fraction of coarse hyper-fluorescent particle number concentrations to total coarse particles vs. different marine microbe measurements

S7.6 Hyper-fluorescent particle number concentration fraction vs OM measurements

Figure S17 shows the results of fraction of coarse fluorescent particle number concentrations to total coarse particles against OM measurements. Fits are analogue to S 9.1.ss

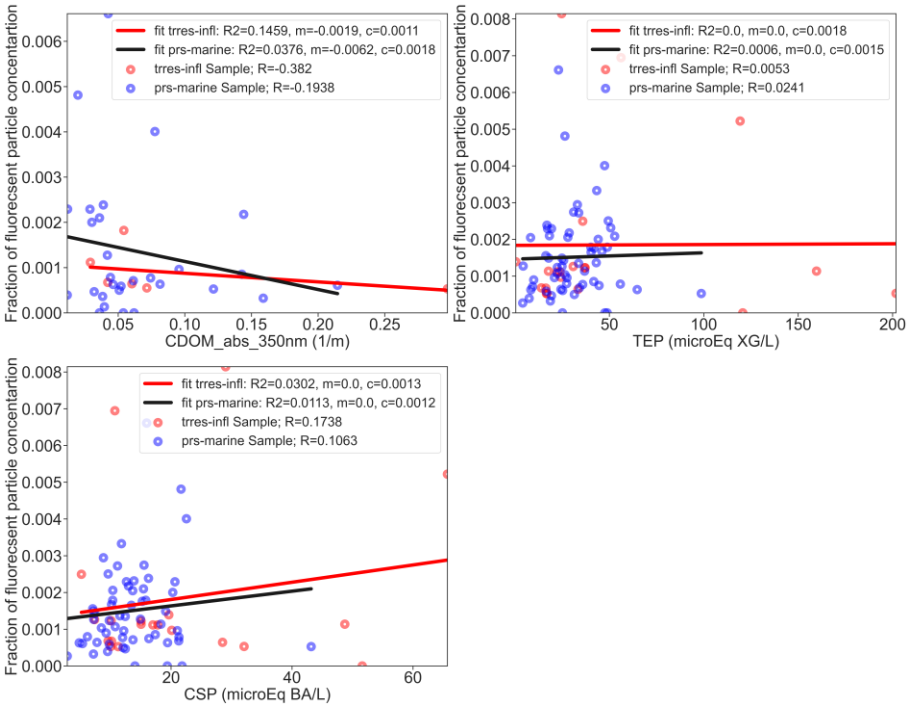

267

268 **Figure S17.** Scatter plot of fraction of coarse hyper-fluorescent particle number
269 concentrations to total coarse particles vs. OM measurements

270 **Text S8: p value results of marine measurement**

271 The p values for the marine varibales used in the correlation study against (hyper-

272 fluorescent particles) are demonstrated in Figure S18.

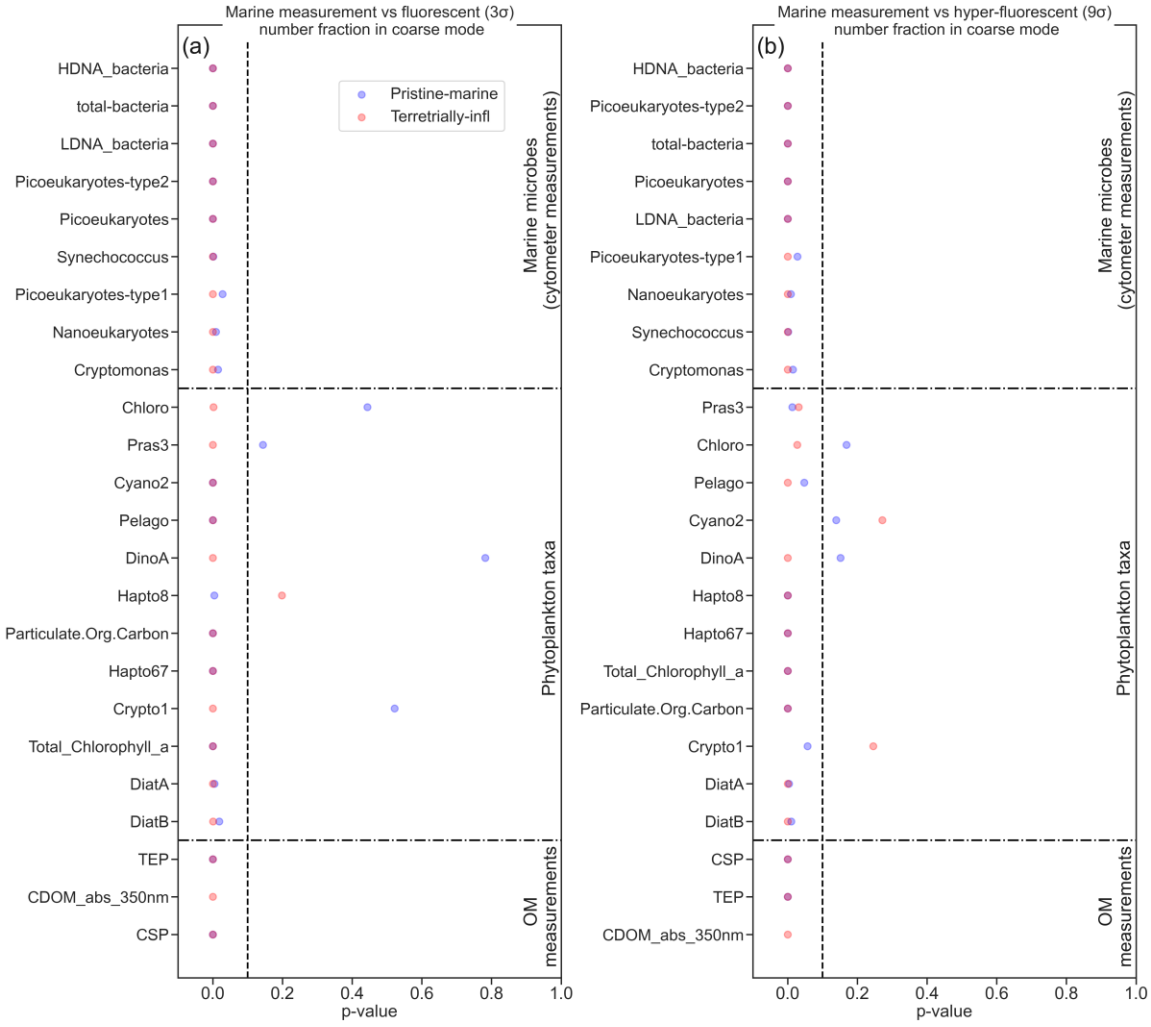

Figure S18. (a) p values of marine variables against fluorescent aerosols, and (b) p values of marine variables against hyper-fluorescent aerosols.

Text S8: Subsampling analysis of fluorescent type classification

S.8.1 Variation of the fluorescent type fraction of pristine-marine segment samples based on 24 hour random data points subsampling

Figure S.19 to S.21 demonstrate the resampling results for segment 1 to 3. Random subsamples of 288 points (equivalent to 24 hours of data) from 5 min time average datasets of fluorescent aerosol measurements from pristine-marine air masses of different segments were drawn. The resampling process was repeated 15 times to

provide a number of resample ensembles to compare their variability with results of full segment data sets.

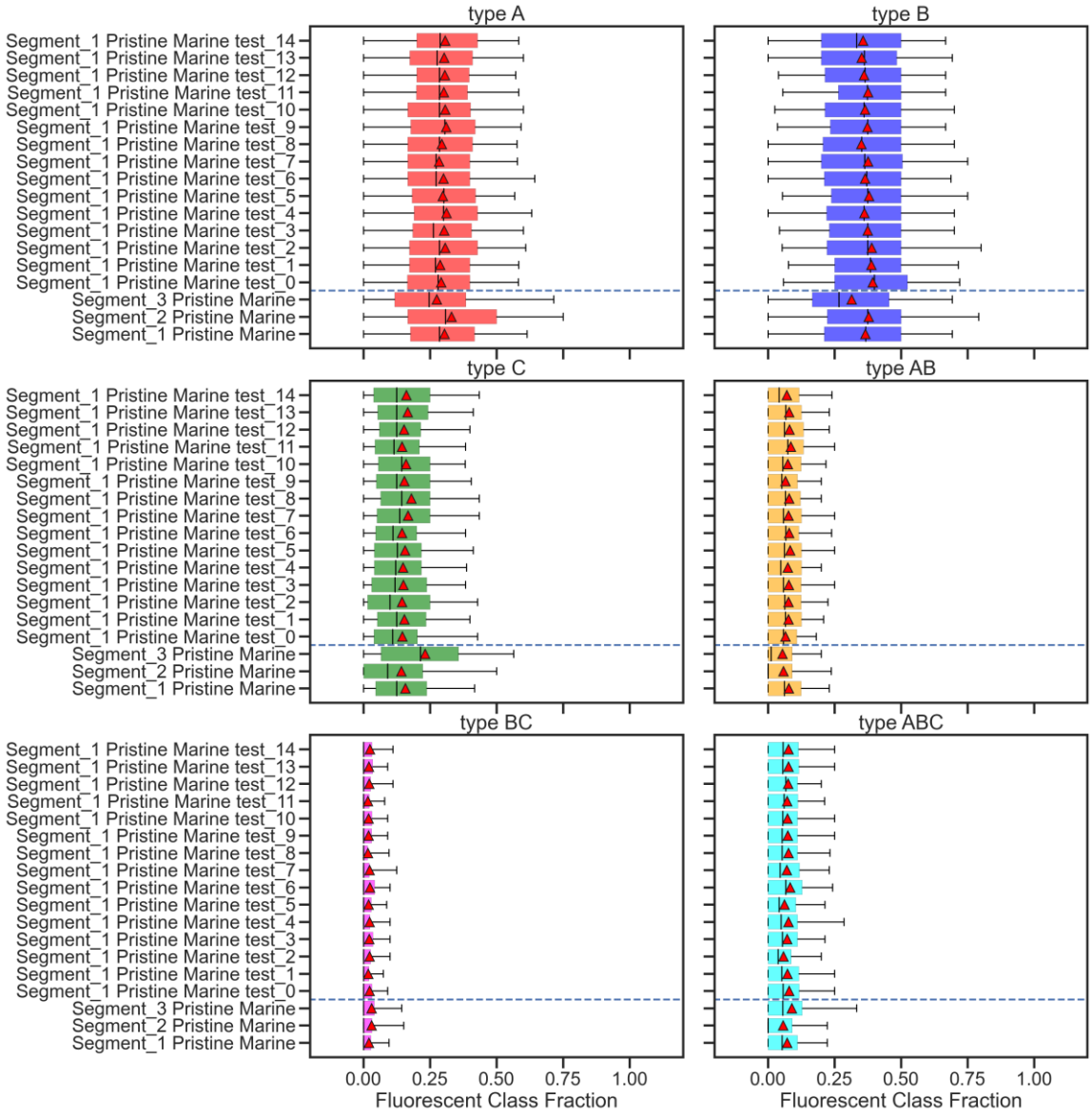

Figure S19. Fluorescent type fraction subsampling results for pristine-marine air masses from segment 1 for coarse fluorescent particles (3σ)

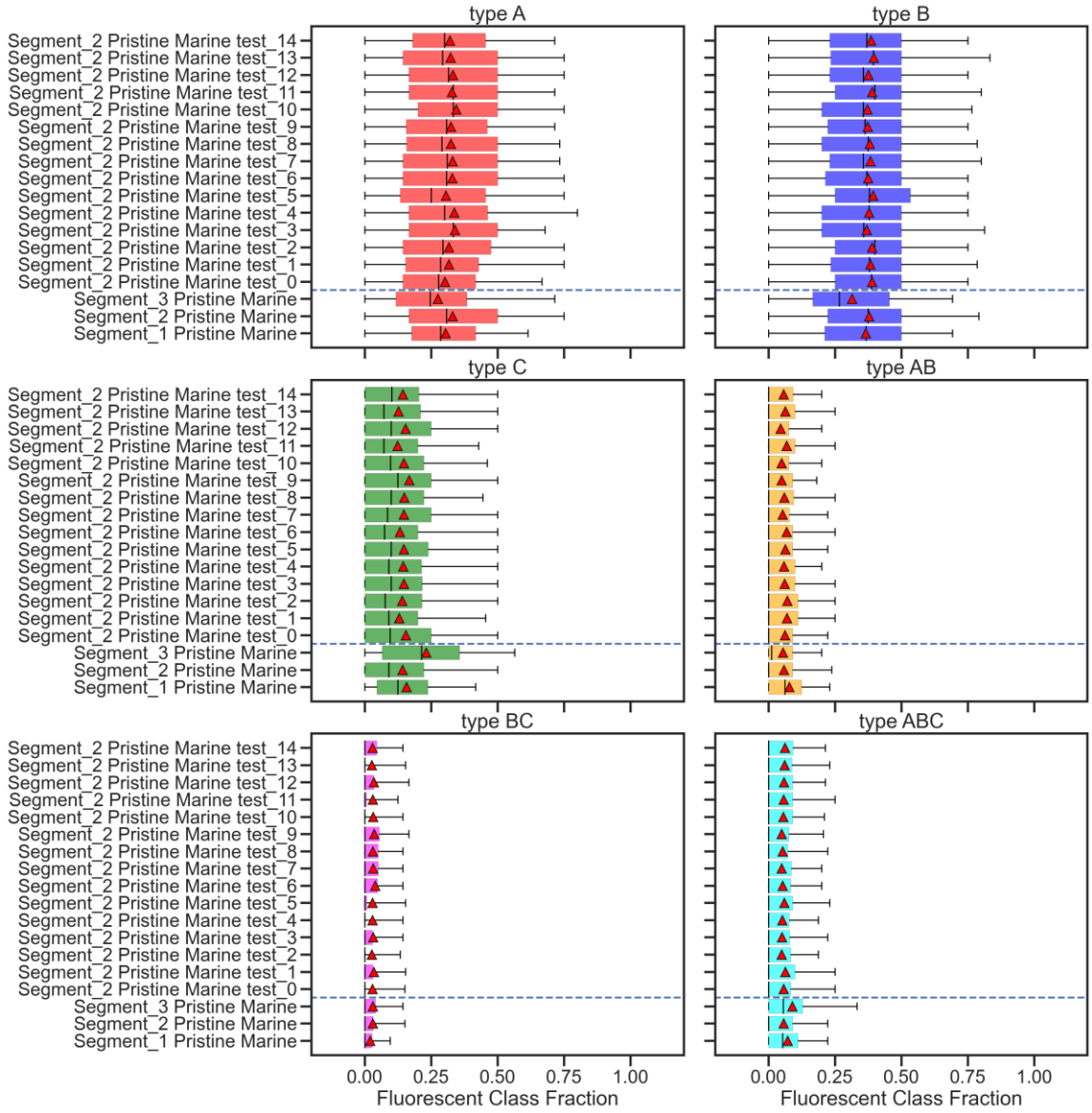

Figure S20. Fluorescent type fraction subsampling results for pristine-marine air masses from segment 2 for coarse fluorescent particles (3σ)

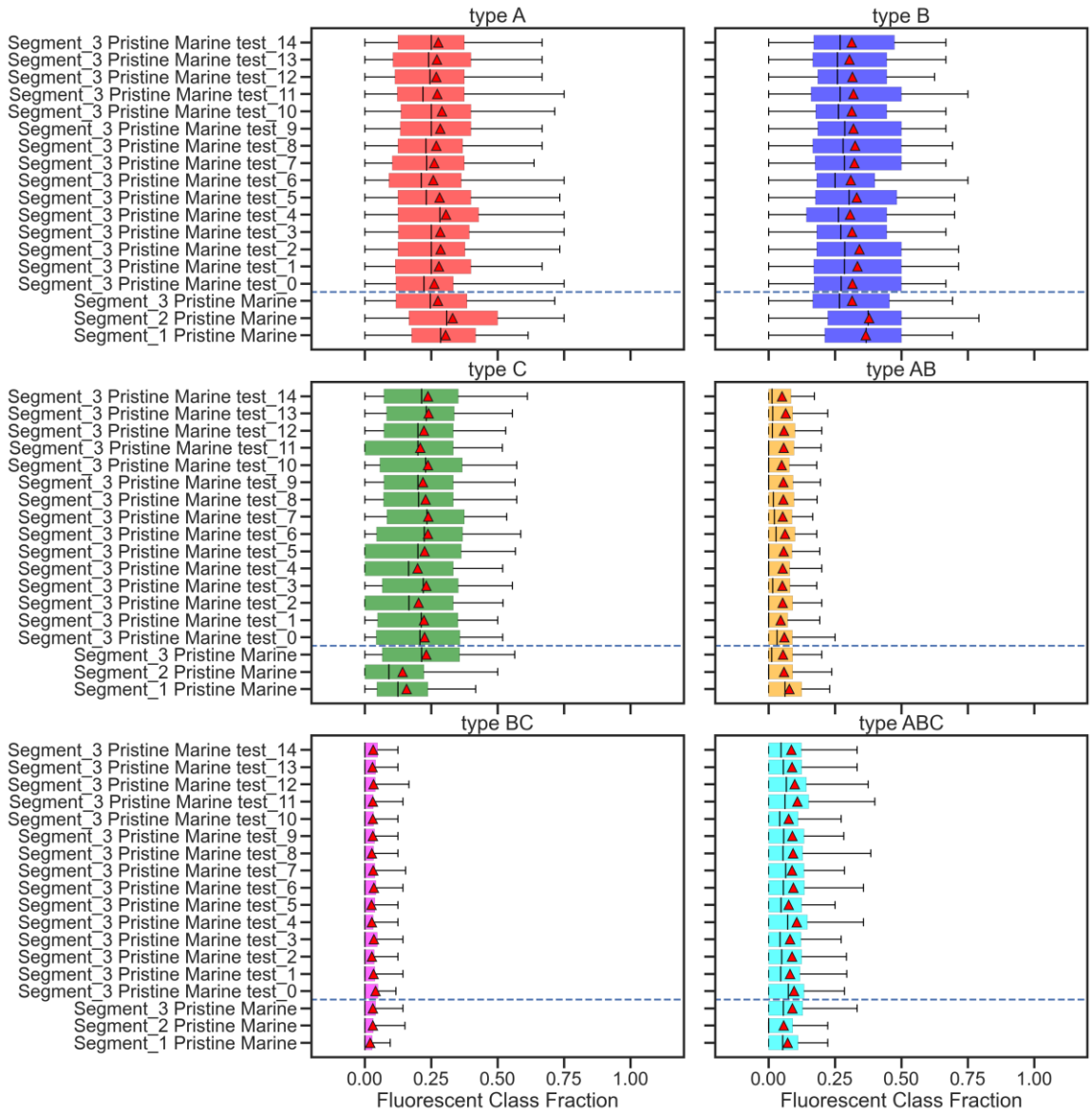

294

295 **Figure S21.** Fluorescent type fraction subsampling results for pristine-marine air masses from
296 segment 3

297

298 ***S.8.2 Variation of fluorescent type fraction based on a constant time window of 24 hours***

299 To investigate the variability of fluorescent type fraction of pristine-marine air masses

300 of each segment over different time periods, an additional subsampling analysis was

301 conducted by drawing subsamples from a fixed time interval of 24 hours. Figure S.22

to S.24 demonstrate the resampling results for segment 1 to 3. For this analysis, in each segment 15 different and randomly selected time intervals were used. Only time intervals containing a total number of data points equivalent to or longer than 12 hours within the 24 hours were considered.

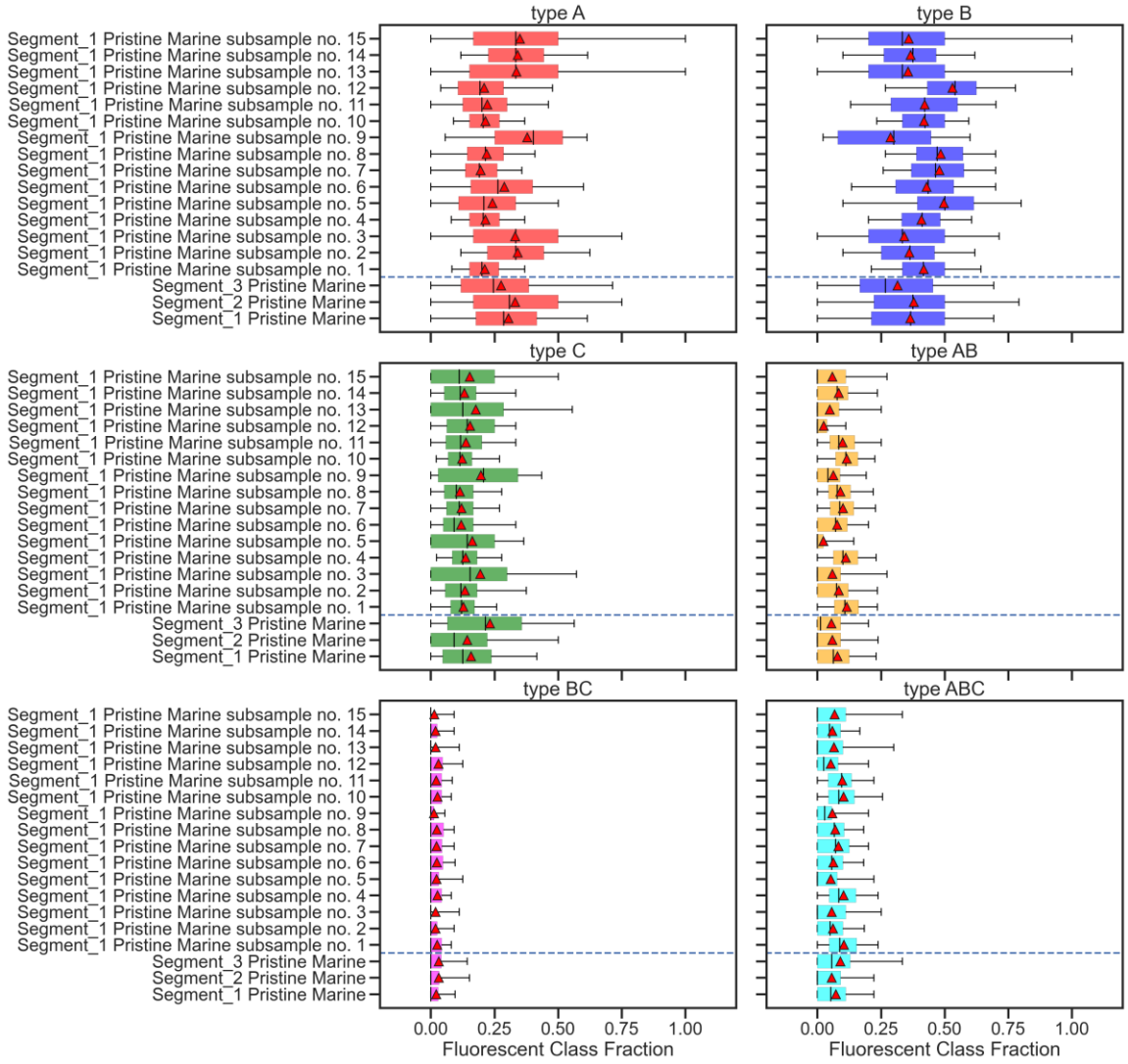

Figure S22. Results of fluorescent type fraction subsampling (based on fixed time windows) results for pristine-marine air masses from segment 1 for coarse fluorescent particles (3σ)

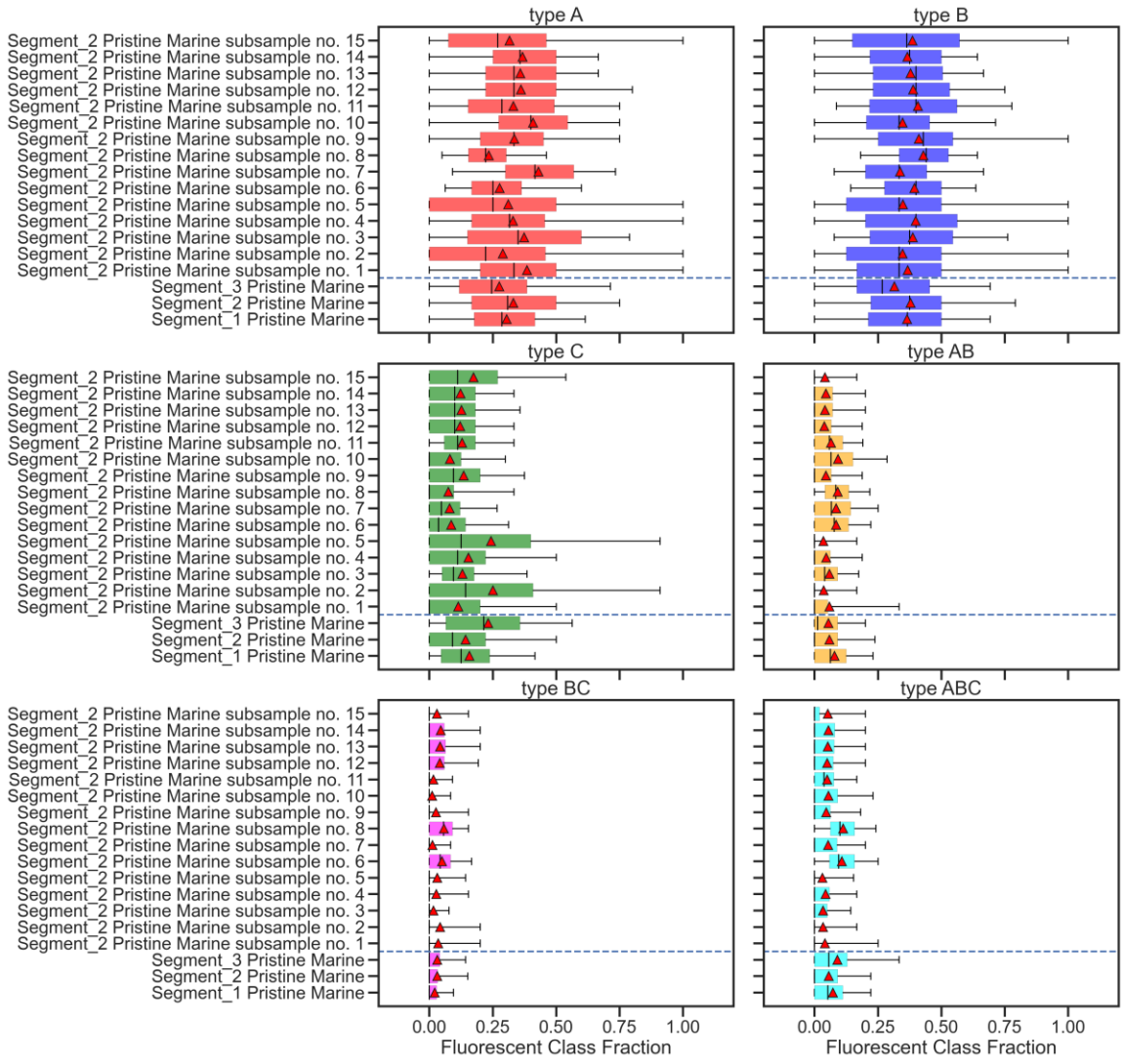

Figure S23. Results of fluorescent type fraction subsampling (based on fixed time windows) results for pristine-marine air masses from segment 2 for coarse fluorescent particles (3σ)

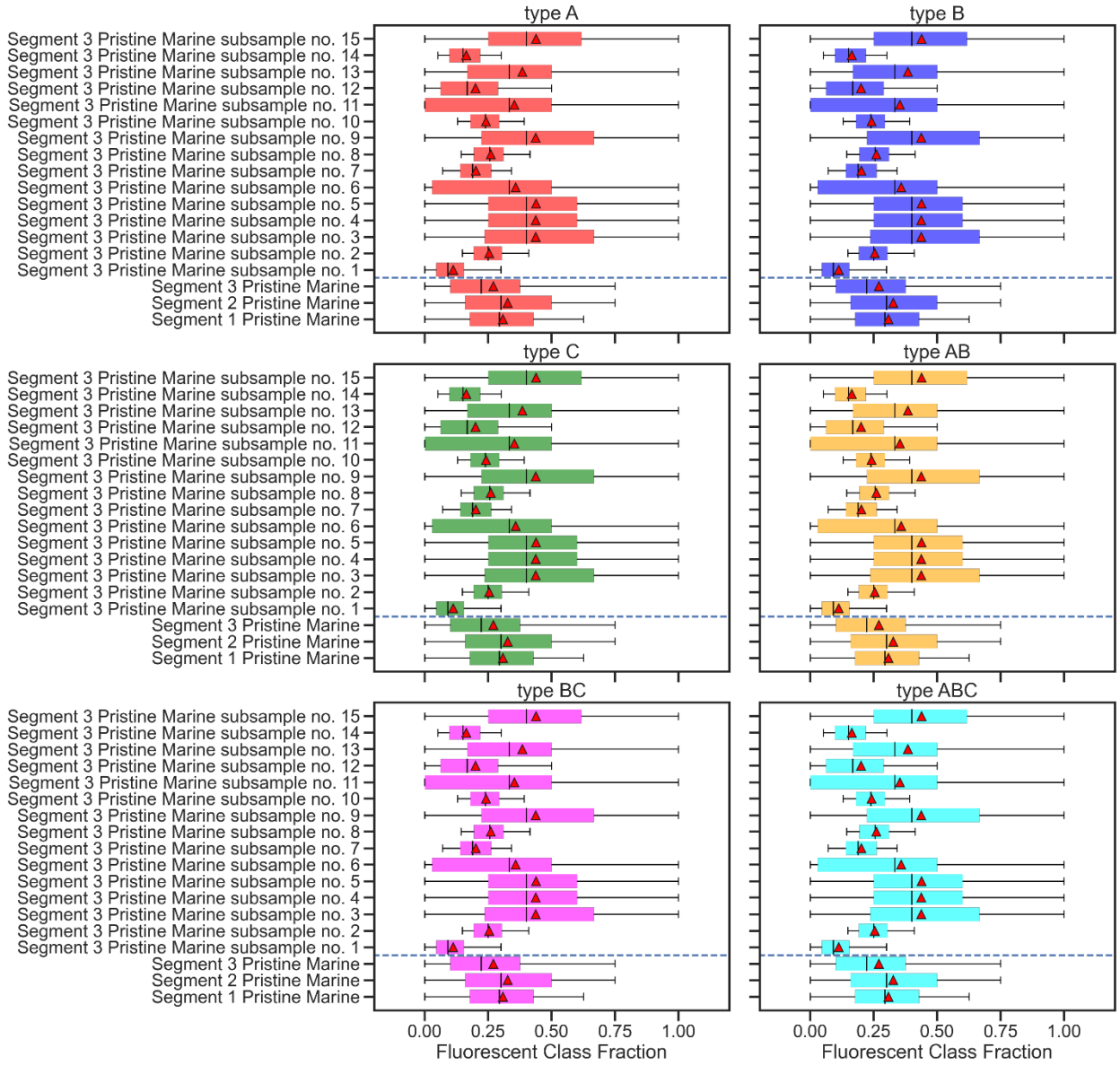

Figure S24. Results of fluorescent type fraction subsampling (based on fixed time windows) for pristine-marine air masses from segment 3 for coarse fluorescent particles (3σ)

Text S9: Average size distribution of aerosol fluorescent classes

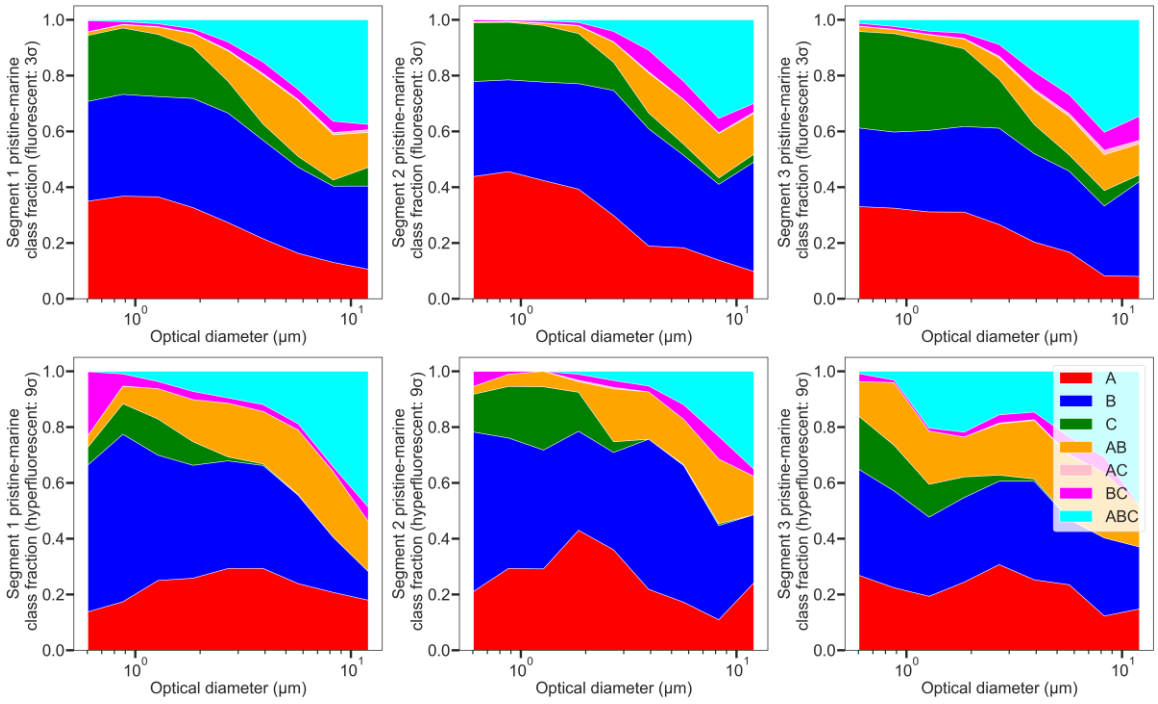

Figure S25. Size distribution of fluorescent type fraction for fluorescent particles (3σ) (top row) and hyper-fluorescent particles (9σ) bottom row for pristine-marine air masses from segment 1 to 3

Text S10: Asymmetry Factor (AF)

Once aerosols are illuminated by the continuous 635 nm laser beam of the WIBS, their forward scattering is measured by a quadrant detector. The quadrant detector has four sensors, which measure a portion of the scattered light intensities. The asymmetry factor is obtained by combining these four measured light intensities through the following formula introduced by Gabey et al. (2010) and used in other studies (Savage et al. 2017):

$$AF = \frac{k(\sum_{i=1}^{n}(E - E_i)^2)^{\frac{1}{2}}}{E}$$ Equation S1

In Eq S1, k is an instrument constant, E is the mean forward scattering signal measured by all the detector sensors, and E_i the scattering signal detected by an individual sensor and n is the number of sensors.